Available online at www.sciencedirect.com
SCIENCE DIRECT
Polymer 47 (2006) 5035–5043
polymer
www.elsevier.com/locate/polymer

Crystallization behavior of star-shaped poly(ethylene oxide) with cubic silsesquioxane (CSSQ) core

K.Y. Mya, K.P. Pramoda, C.B. He *

Molecular and Performance Materials, Institute of Materials Research and Engineering, 3 Research Link, Singapore, Singapore 117602

Received 16 December 2005; received in revised form 16 March 2006; accepted 4 April 2006
Available online 5 June 2006

Abstract

The crystallization behavior of well-defined star-shaped cubic silsesquioxane–poly(ethylene oxide) (CSSQ–PEO) and linear PEO were studied in terms of differential scanning calorimetry (DSC) and wide-angle X-ray scattering (WAXS). It was found in DSC analysis that the glass transition temperature (T_g) and the crystallization temperature (T_c) of CSSQ–PEO are different from those of linear PEO. The presence of CSSQ in PEO reduced the overall crystallization growth rate. This effect can be ascribed to the reduction of the mobility of the PEO crystallites in the presence of CSSQ and the star structure of the polymer. The Ozawa method is qualitatively satisfactory for describing the nonisothermal crystallizations of linear PEO and CSSQ–PEO. The presence of CSSQ leads to the diffusion- and nucleation-controlled mechanisms in the crystallization process of CSSQ–PEO whilst only the nucleation-controlled mechanism was observed in the case of linear PEO. The apparent activation energy required for crystallization was calculated using the Kissinger method. The isothermal crystallization morphology of PEO and CSSQ–PEO were also examined by cross-polarizing optical microscopy (CPOM). The CPOM images indicated the spherulite growth is slower in CSSQ–PEO as compared to linear PEO. It was also investigated that more number of PEO spherulites in CSSQ–PEO were observed, which sizes are markedly smaller than the spherulites developed in linear PEO. Wide-angle X-ray scattering (WAXS) studies showed that the crystallization peaks for linear PEO and CSSQ–PEO appeared at different temperature revealing the crystallization process and crystal growth rate are different from each other. However, no significant distortion of the crystal structure of PEO was evaluated in the presence of CSSQ.

Keywords: Cubic silsesquioxane (CSSQ); Star-shaped cubic silsesquioxane–poly(ethylene oxide) (CSSQ–PEO); Crystallization

1. Introduction

In the past decade, studies on the crystallization behavior of polymers are mainly interested in the isothermal processes [1–5]. In practice, most polymers and nanocomposites are processed in extrusion, melt spinning, and injection molding under nonisothermal conditions [6]. Therefore, many recent works have addressed the study of the nonisothermal crystallization behavior of polymers and blends [7–10]. In addition, macromolecules containing inorganic materials have attained much attention in the past decades due to their potential candidates for the inorganic–organic hybrid materials. The crystallization behavior of polymer with inorganic materials has been extensively studied [11–13]. Strawhecker and Manias [11] found the enhancement in overall crystallization rate of poly(ethylene oxide) (PEO) in the presence of inorganic filler (sodium montmorillonite). On the other hand, its crystallization is inhibited by Na^+ cations, showing the decrease in spherulite growth rate and crystallization temperature. These two mechanisms are simultaneously present in PEO with Na^+ MMT inorganic filler. Lee et al. [12] reported the crystallization behavior of poly(caprolactone) (PCL)/poly(vinyl butyral) (PVB) blend containing inorganic filler (carbon black). It was shown that the carbon black does not affect on the spherulite growth rate of PCL homopolymer. On the other hand, the growth rate is dependent on the PVB content in PCL/PVB blend, regardless of the carbon black content. This indicated that the crystallization behavior and spherulite growth rate are strongly influenced on the composition of the polymer and the different polymeric systems.

The cubic silsesquioxanes (CSSQ) have been found to offer attractive properties that include improved thermal stability, chemical resistance, and enhancements in mechanical properties [14–17]. The structure of CSSQ has been demonstrated to be a nanosized inorganic silica core surrounded by the organic functional groups on the silica surface with the diameter between 0.7 and 1.5 nm [18–21]. Therefore, the CSSQ

* Corresponding author. Tel.: +65 68748145; fax: +65 68727528.
E-mail address: cb-he@imre.a-star.edu.sg (C.B. He).

0032-3861/$ - see front matter © 2006 Elsevier Ltd. All rights reserved.
doi:10.1016/j.polymer.2006.04.068

macromonomers can be used as building blocks for the construction of inorganic–organic nanosized hybrid materials [22,23]. Since, poly(ethylene oxide) (PEO) has many technological and industrial applications, the incorporating of PEO onto CSSQ is of particular interest. Kim and Mather [24] reported the synthesis and characterization of amphiphilic telechelics PEG end-capped with CSSQ. The hydrophobicity of CSSQ was modified by using a different molecular weight of PEG. The modification to the crystallization behavior of PEG was observed in the presence of monosubstituted CSSQ macromonomer due to the bulkiness of CSSQ groups with respect to crystalline lamellae dimensions. Different thermal and morphological properties were observed by controlling the balance of the hydrophilic PEG and the hydrophobic CSSQ macromonomer. The synthesis and thermal properties of oligomeric poly(ethylene oxide)–functionalized silsesquioxanes were also reported by Maitra and Wunder [25]. Their studies showed how the thermal behavior of PEO was influenced by the silica surface of CSSQ. The mobility of the PEO chain is reduced as observed by an increase in the glass transition temperature (T_g) due to interfacial effect and suppression in crystallization compared to linear materials. Recent molecular dynamics simulation studies [26–28] have reported the effect of CSSQ on polymer motion analyzed through the mean square displacement function. Their results showed that the presence of CSSQ moieties retard the motion of the polymer chain.

In our previous paper, we have reported the synthesis and aggregation behavior of well-defined star-shaped amphiphilic CSSQ–PEO in aqueous solution [29]. The star-shaped polymers have also been found to exhibit interesting morphologies and viscoelastic properties significantly different than that of their linear counterparts [30,31]. Since, most polymers and nanocomposites are processed under nonisothermal conditions, it is of great interest to study the nonisothermal crystallization kinetics of well-defined star-shaped CSSQ–PEO by DSC analysis. The kinetics data are analyzed by Avrami and Ozawa methods for nonisothermal crystallization. The required activation energies for crystallization are evaluated by the well-known Kissinger method. As a comparison, the nonisothermal crystallization of commercially available monomethyl ether terminated poly(ethylene oxide) (referred as linear PEO) is also studied by DSC analysis. The crystallographic changes occurred in both PEO and CSSQ–PEO are studied by WAXS analysis during nonisothermal crystallization from the melt. In addition, the changes in crystallization morphology during isothermal crystallization condition of linear PEO and CSSQ–PEO are examined via cross-polarizing optical microscopy (CPOM).

2. Experimental

2.1. Materials

Poly(ethylene oxide) methyl ether (M-PEO) with average molecular weight of 2000 was purchased from Sigma–Aldrich and used as received. It is denoted as linear PEO throughout the text. Allyl bromide (Aldrich) was used for the preparation of allyl terminated monomethyl PEO (allyl-PEO). A 10 wt% aqueous solution of methylammonium hydroxide (Aldrich), dimethylchlorosilane (Aldrich), and Tetraethoxysilane (Aldrich) were used for the synthesis of CSSQ, namely, octakis (dimethylsiloxy) octasilsesquioxane ($Q_8M_8^H$) without further purification. Platinum divinyltetramethyl disiloxane Pt(dvs) catalyst was obtained from Aldrich Co. and diluted to 2 mM solution in anhydrous toluene.

2.2. Synthesis of CSSQ–PEO

Allyl terminated monomethyl PEO (allyl-PEO) was prepared according to the literature procedure [32]. The octakis (dimethylsiloxy) octasilsesquioxane ($Q_8M_8^H$) was prepared by

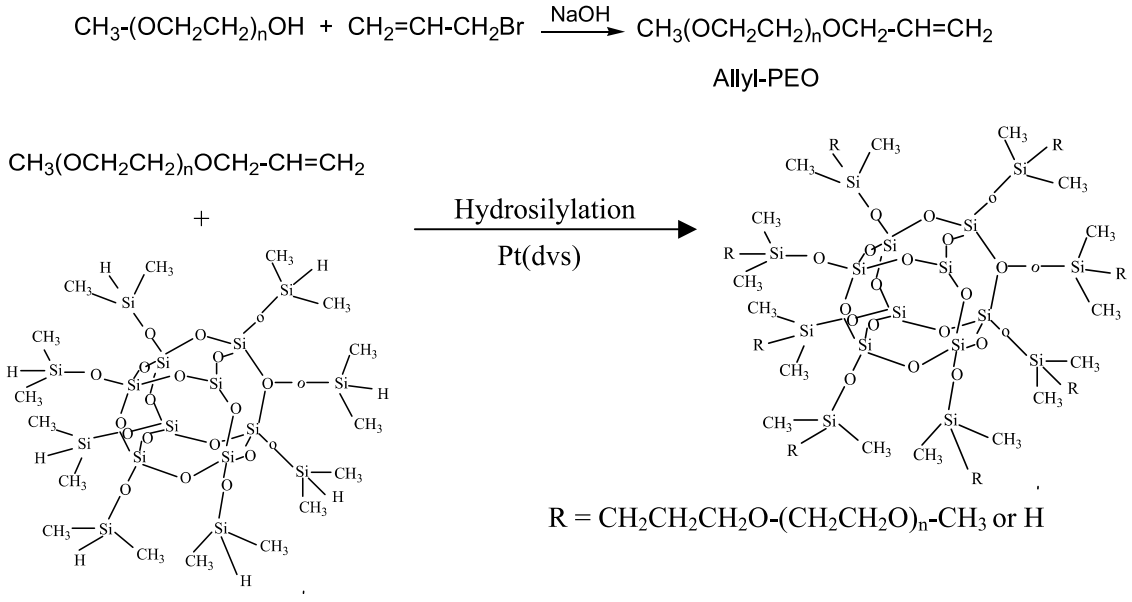

Fig. 1. Synthesis procedure of CSSQ–PEO.

the literature method [33,34]. The CSSQ–PEO was synthesized by a hydrosilylation reaction as shown in Fig. 1. The detailed procedure was described in our previous paper [29]. In a typical synthesis, $Q_8M_8^H$ (0.50 g, 0.49 mmol) and 9.80 g (4.90 mmol) of allyl-PEO were dissolved into dried toluene in a two-necked flask equipped with a reflux condenser and a magnetic stirrer. Pt(dvs) (~3 mL) was added as a catalyst after the complete dissolution of $Q_8M_8^H$ and allyl-PEO in toluene. The mixture was then stirred for 20 h at 85 °C under an argon atmosphere. The final product was isolated and purified by repeated fractionation in an anhydrous ether and methanol mixture. The well-defined structure of star-shaped CSSQ–PEO was characterized by using ^{1}H NMR, FTIR, and GPC techniques.

^{1}H NMR (400 MHz, $CDCl_3$, δ: ppm): 0.16 [Si(CH_3)$_2$$CH_2$–], 0.63 (Si$CH_2$$CH_2$$CH_2$O), 1.29 (Si$CH_2$$CH_2$$CH_2$O), 1.75 (Si$CH_2$-$CH_2$$CH_2$O), 3.40 (–O$CH_3$), 3.65 (–$CH_2$$CH_2$O–).

FTIR (cm^{-1}, KBr pellet): 1120 (ν Si–O–Si; δ C–H), 960 (δ Si–CH_3; δ C–O), and 840 (δ Si–CH_2; ν C–O). GPC: M_n = 11,650; M_w = 12,950; M_w/M_n = 1.11.

2.3. Characterizations

Differential scanning calorimetry (DSC) measurements were performed using a TA Instrument DSC 2920 equipped with the RCS cooling system. The nonisothermal crystallization process of the linear PEO and CSSQ–PEO samples were carried out in various cooling rates (2.5, 5, 10, 20 °C/min) under a nitrogen atmosphere. All samples were sealed in aluminum pans before measurement. To avoid thermal history, each sample was first heated from −40 to 60 °C and maintained at this temperature for 5 min and the data were collected from the second cooling cycle. The relative degree of crystallinity can be defined as

$$X_t = \frac{\int_{T_0}^{T} (\mathrm{d}H_c/\mathrm{d}T)\mathrm{d}T}{\int_{T_0}^{T_\infty} (\mathrm{d}H_c/\mathrm{d}T)\mathrm{d}T} \quad (1)$$

where X_t is the relative degree of crystallinity, T_0 and T_∞ are the initial and end crystallization temperatures, $\mathrm{d}H_c$ is the enthalpy of crystallization. The crystallization kinetics of PEO and CSSQ–PEO are described by the Avrami equation [35]

$$1 - X_t = \exp(-kt^n) \quad (2)$$

where k is the crystallization rate constant, t is the time, and n being the Avrami exponent relating to the type of nucleation and growth. Generally, the exponent n should be a value between 1 and 4 depending on the different crystallization mechanism. However, the Avrami parameters n and k have different physical meanings in nonisothermal crystallization because the temperature changes constantly during nonisothermal condition.

Ozawa [36] modified the Avrami equation to describe the nonisothermal crystallization kinetics as follows

$$1 - X_t = \exp[-\varphi(T)/\beta^m] \quad (3)$$

where $\phi(T)$ is the cooling function of the crystallization process, β is the cooling rate, and m is the Ozawa exponent depending on the dimension of the crystal growth. The exponent m and $\phi(T)$ can be determined from the slope and intercept coefficients of the plot of $\ln[-\ln(1-X_t)]$ versus $\ln\beta$ at a fixed temperature.

The cross-polarizing optical microscopy was carried out using a heating stage (Linkam THMS-600) of a polarizing light microscope (PLM, Nikon) connected to a video camera. The temperature was raised to 40 °C/min and the time measurement was started when the desired temperature was reached. The crystallization process was observed in situ by PLM with crossed polarizers and the micrographs were recorded in real time video for further analysis.

Wide angle X-ray scattering (WAXS) was performed using a Bruker AXS General Area Detector Diffraction System (GADDS). The applied voltage and current were 40 kV and 40 mA, respectively. The samples were mounted on aluminum holder and scanned from 2 to 40° 2θ. The well-known Bragg's equation ($\lambda = 2d \sin\theta$) [37] was used to calculate the d spacing, where λ is a wavelength: 0.154 nm, d is the distance between each adjacent crystal plane (d-spacing), and θ is the Bragg angle.

3. Results and discussion

Fig. 2 shows the DSC heating and cooling thermograms for linear PEO and CSSQ–PEO measured at a heating (cooling) rate of 10 °C/min. The exothermic peaks represent for crystallization and the endotherms correspond to the melting of linear PEO and CSSQ–PEO.

The relatively narrow melting temperature (T_m) of CSSQ–PEO is observed compared to that of PEO homopolymer and the appearance of the single melting transition for linear PEO attributed to the absence of folded PEO chain [38]. The crystallization temperature (T_c) of PEO decreases when PEO incorporated with CSSQ. This implies the crystallization of PEO becomes slower in the presence of CSSQ. The glass transition temperature (T_g), T_c, and the melting temperature

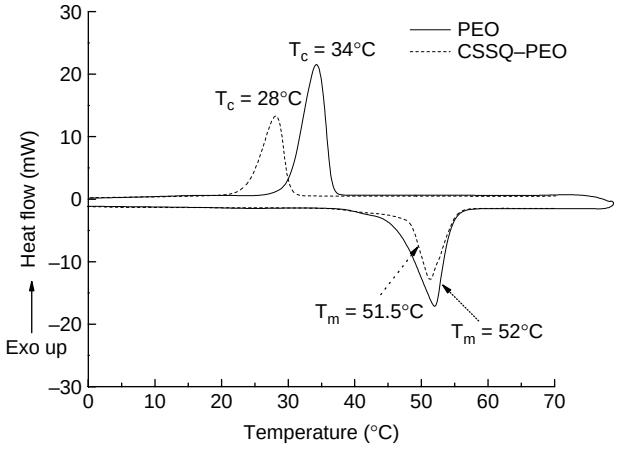

Fig. 2. The crystallization isotherms and the melting behavior of PEO and CSSQ–PEO at cooling (heating) rate 10 °C/min.

Table 1
The glass transition, melting, crystallization temperatures, and the percent crystallinity of linear PEO and CSSQ–PEO

Sample	T_g (°C)	T_m (°C)	T_c (°C)	Crystallinity (%)
PEO	−34.0	52.0	34.0	86.2
CSSQ–PEO	−25.0	51.5	28.0	58.1

(T_m) of linear PEO and CSSQ–PEO are listed in Table 1. The single T_g exhibits only one component in the CSSQ–PEO and the T_g of PEO increases from −34 to −25 °C in the presence of CSSQ. It is believed that the rigid CSSQ core hinders the mobility of PEO chain and provides the improved thermal stability of PEO. This interpretation is supported by the molecular dynamics simulation studies [26–28,39]. Their studies reported the CSSQ moieties are confined to a cage formed by the surrounding polymer chains and performs non-diffusive motions within the CSSQ cage. The segmental motion of PEO was hindered by the inorganic phase and the cooperative motion decreased by the segments immobilized by interactions with CSSQ. On the other hand, T_m is not much affected on the addition of CSSQ due to the small component compared to PEO. As shown in Table 1, the decrease in T_c of PEO is observed in the presence of CSSQ. It is clearly showed that the attachment of CSSQ in PEO results in a decrease of crystallization temperature. A similar decrease in crystallization temperature was also observed when poly(ethylene oxide)/polyamide reinforced with montmorillonite clay [7,11]. The percent crystallinities of linear PEO and star structure of CSSQ–PEO were determined using the following equation

$$\text{Crystallinity (\%)} = \frac{\Delta H_m - \Delta H_c}{\Delta H_m^0} \times 100\% \quad (4)$$

where ΔH_m and ΔH_c are the melting and recrystallization enthalpy (J/g) and ΔH_m^0 represents the standard melting enthalpy of perfect PEO crystal (188.9 J/g) [40]. Here, we assume the same perfect crystallization enthalpies for PEO and CSSQ–PEO and evaluated the percent crystallinity of both PEO and CSSQ–PEO according to Eq. (4). As seen in Table 1, the percent crystallinity of the linear PEO decreases from 86.2 to 58.1% in the presence of CSSQ forming the star-shaped structure of CSSQ–PEO.

3.1. Nonisothermal crystallization behavior of PEO and CSSQ–PEO

The maximum and onset peak crystallization temperatures ($T_{c,max}$ and $T_{c,onset}$) of PEO and CSSQ–PEO at different cooling rate are shown in Fig. 3. The value of T_c decreases with increasing cooling rate and the incorporation of CSSQ into PEO is dropped T_c by 5–6 °C, indicating that the cubic structure of CSSQ obstructs the crystallization of PEO. The dependence of T_c on cooling rate for linear PEO exhibits the similar trend with CSSQ–PEO as shown in Fig. 3. This observation is consistent with the literature [11], which studied the crystallization behavior of PEO in the addition of sodium montmorillonite filler. It was shown that the addition of montmorillonite filler inhibited the PEO crystallization and manifested in the decrease of the crystallization temperature.

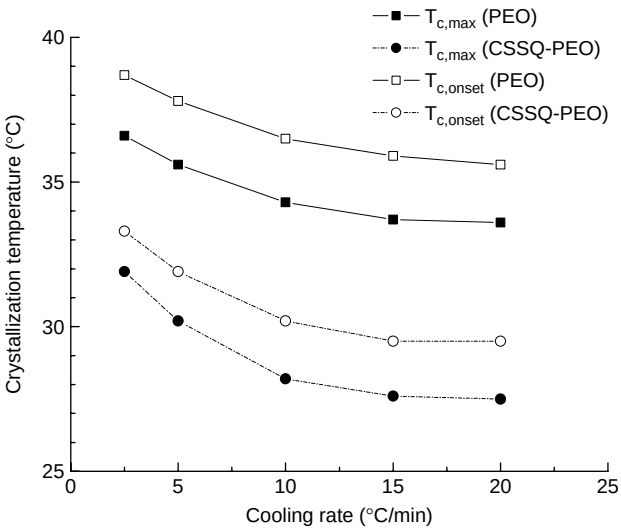

Fig. 3. The plot of crystallization temperature versus cooling rate for PEO and CSSQ–PEO.

The relative degrees of crystallinity (X_t) as a function of crystallization temperature for linear PEO and CSSQ–PEO at various cooling rates are plotted in Fig. 4. It is observed that the peak crystallization temperature of PEO and CSSQ–PEO decrease as increasing cooling rate. All curves in Fig. 4(a) and (b) show reverse sigmoidal shape, suggesting that the crystal nucleation takes place from the melt and slow down during the nucleation growth. In Fig. 4(b), the crystallization of CSSQ–PEO is slower in the later stage compared to that of linear counterpart due to the steric hindrance of CSSQ during PEO crystallization.

The nonisothermal crystallization kinetics of linear PEO and CSSQ–PEO were studied by Avrami (Eq. (2)) and Ozawa (Eq. (3)) methods. Fig. 5 shows the Avrami plot, $\ln[-\ln(1-X_t)]$ versus $\ln t$, for linear PEO and CSSQ–PEO at different cooling rates. It is found that the linear regressions fit only in the early stage of crystallizations and deviations occur in the late crystallizations for linear PEO and CSSQ–PEO. This observation is different from the crystallization kinetics of PEO in PET–PEO copolymer as reported in the literature [41]. Their analysis showed the crystallization behavior of PEO-6000 obeys the Avrami model. However, the deviation of the Avrami plot was observed for PEO in PET–PEO copolymer because a large portion of the crystallization was attributed to the secondary process. In the present study, the failure of the Avrami model may be due to the low molecular weight PEO (∼2000) that affects on the crystallization behavior. The time required for the completion of the crystallization process for low molecular weight will be faster compared to the high molecular weight. Another reason for the failure of the Avrami equation is due to the fact that the temperature changes constantly under nonisothermal condition and this constant change influences on the nucleation and spherulite growth rate. Beech et al. [42] reported that the deviation in the Avrami equation is due to the different secondary processes, which

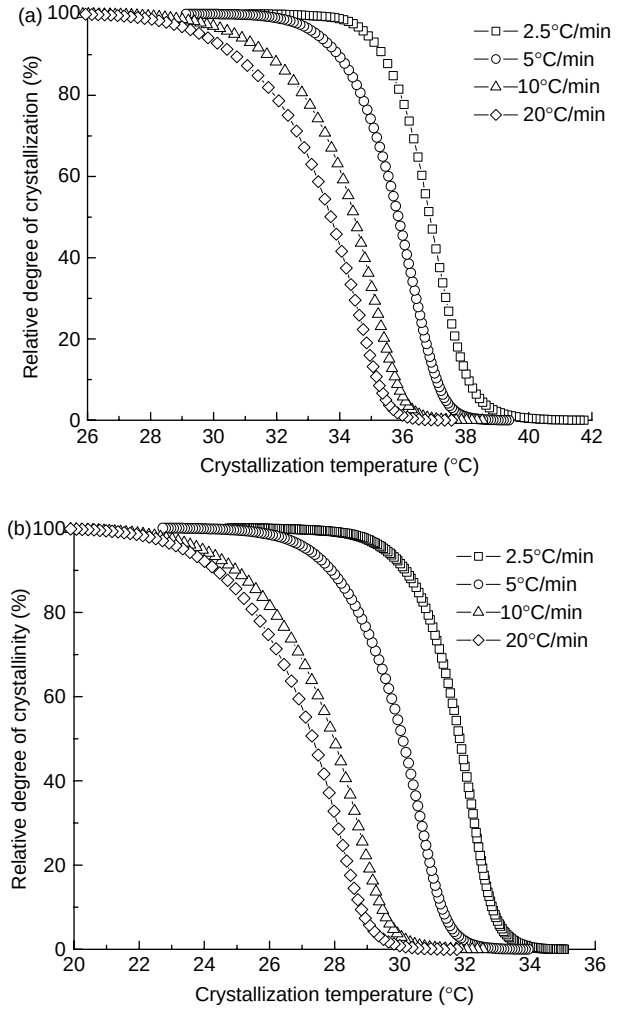

Fig. 4. The relative degree of crystallinity (X_t) as a function of crystallization temperature for (a) linear PEO and (b) CSSQ–PEO at various cooling rates.

depend on the molecular weight. It was found that there is a fractionation by molecular weight with attenuation in crystallization rate as crystallization proceeds for polymers with low molecular weight (<6000). Godovsky et al. [43] also reported the temperature dependence of the spherulites growth rate and the crystallization kinetics of PEO in the molecular weight range of 300–20,000 and found that both growth rate and the crystallization kinetics depend on the molecular weight. It is observed, in this study, that the low molecular weight of PEO (2000) crystallizes faster (~1–2 min) compared to the large molecular weight reported in the literatures (PEO-6000 and PEO-100,000) [41,44]. Although CSSQ–PEO has large molecular weight (~13,000 measured by GPC), each PEO chain attached to the vertex of the cage structure of CSSQ exhibiting the star-shaped CSSQ–PEO. In this case, Avrami model does not adequately describe the nonisothermal crystallization kinetics of PEO and CSSQ–PEO. Since, Avrami equation is inappropriate to describe the nonisothermal condition, attempts were made by using Ozawa analysis.

Fig. 6 shows the nonisothermal crystallization kinetics of PEO and CSSQ–PEO using Ozawa method. Data analysis was carried out from the plots of $\ln[-\ln(1-X_t)]$ versus $\ln \beta$ within

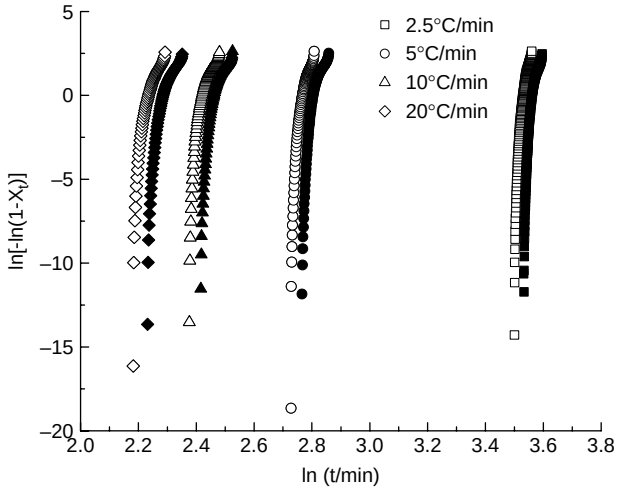

Fig. 5. The plot of $\ln[-\ln(1-X_t)]$ versus $\ln t$ for linear PEO (open symbols); and CSSQ–PEO (closed symbols) at different cooling rate.

the crystallization temperature range of 29–37 °C for neat PEO and 23–31 °C for CSSQ–PEO, respectively. Qualitatively, the Ozawa method is satisfactory for describing the nonisothermal crystallizations of PEO and CSSQ–PEO as shown in Fig. 6. It

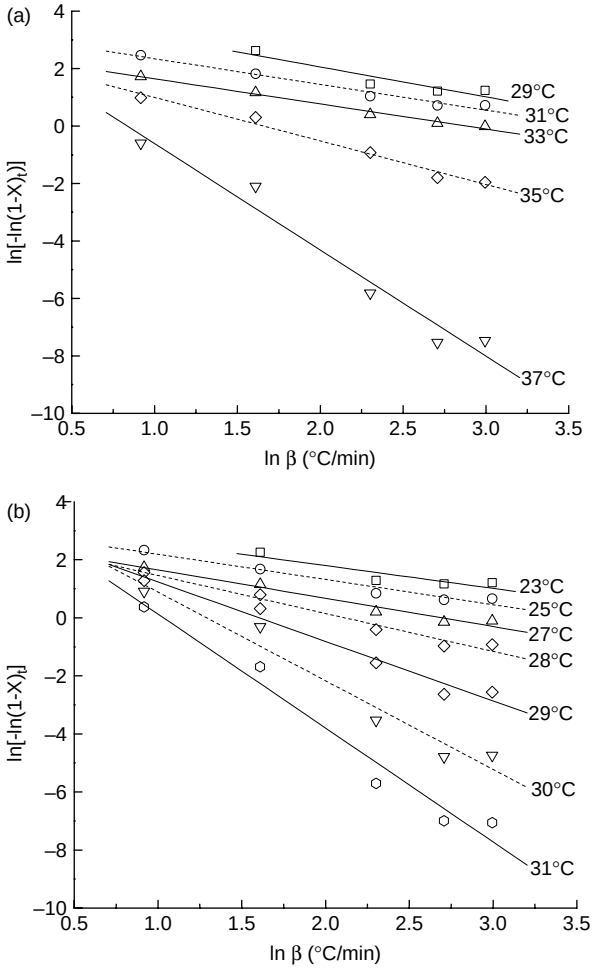

Fig. 6. Ozawa method for linear PEO (a) and CSSQ–PEO (b) at different crystallization temperature.

Table 2
Nonisothermal crystallization kinetics of PEO and CSSQ–PEO analyzed by Ozawa and Kissinger methods

Temperature (°C)	m	$\phi(T)$	ΔE_a (kcal/mol)
PEO			122.8
29	1.04	62.99	
31	0.90	25.52	
33	0.87	12.40	
35	1.50	12.30	
37	3.70	21.88	
CSSQ–PEO			80.4
23	0.78	28.97	
25	0.87	21.22	
27	0.97	13.79	
28	1.31	15.95	
29	2.05	26.78	
30	3.05	51.42	
31	3.92	57.44	

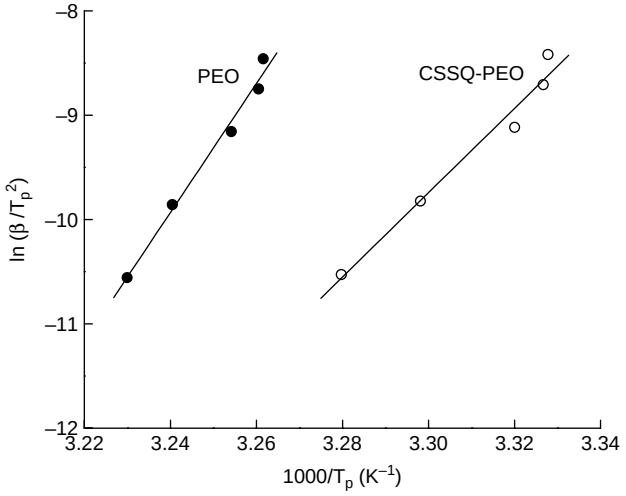

Fig. 7. Kissinger method to evaluate the activation energy of linear PEO and CSSQ–PEO.

is observed that the relative degree of crystallinity strongly depends on the cooling rate at the initial stage of crystallization but slightly affects on the cooling rate at the end of the crystallization process. The kinetic parameters (m and $\phi(T)$) analyzed by Ozawa method are summarized in Table 2. The average values of m are found to be 1.6 ± 1.2 and 1.9 ± 1.2 for PEO and CSSQ–PEO, respectively. The value of $\phi(T)$ for linear PEO decreases with increasing temperature except at the beginning of crystallization, suggesting for the crystallization in the nucleation-controlled region [45]. However, in the system of CSSQ–PEO, it is interesting to note that $\phi(T)$ increases with an increase of temperature in the initial stage of crystallization implying the crystallization process is controlled by the diffusion [46]. The presence of CSSQ cage leads to the diffusion-controlled mechanism in the initial stage whereas it decreases in the final stage of crystallization, as expected for the crystallization in the nucleation-controlled mechanism with slower cooling rate at higher temperature. The PEO segments near the CSSQ core would crystallize in their domains and are restricted to further crystallization resulting in low degree of PEO crystallinity in CSSQ–PEO.

Kissinger [47] proposed a method to evaluate the apparent activation energy for the nonisothermal crystallization at different cooling rate, which can be described by the following equation

$$\frac{\mathrm{d}[\ln(\beta/T_p^2)]}{\mathrm{d}(1/T_p)} = -\frac{\Delta E_a}{R} \tag{5}$$

where β is the cooling rate, T_p is the crystallization peak temperature, ΔE_a is the activation energy of the nonisothermal crystallization process and R being the universal gas constant, respectively. Fig. 7 shows the linear plot of $\ln(\beta/T_p^2)$ against $1/T_p$ for both PEO and CSSQ–PEO and the activation energies were determined from the slopes of the linear regressions and the results are tabulated in Table 2. The ΔE_a for linear PEO is

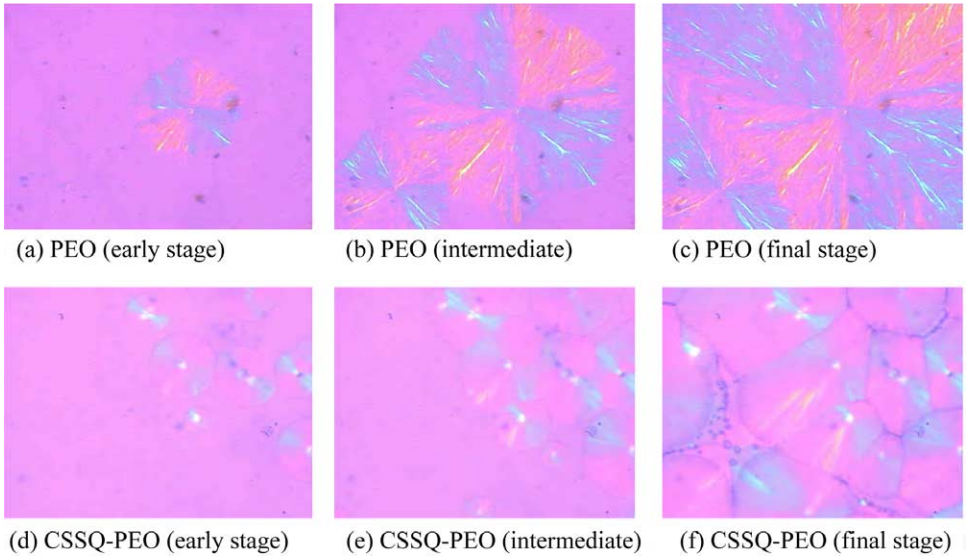

Fig. 8. Polarized light optical images of PEO (a–c) and CSSQ–PEO (d–f) crystallized at 30 °C. Images (a) and (d) are developed in the early stage of crystallization, (b) and (e) are taken in the intermediate stage, and (c) and (f) are the final images. (A colour version of this figure can be viewed in the online issue)

found to be 122.8 kcal/mol, which reduces to 80.4 kcal/mol when incorporating with CSSQ. The activation energies of CSSQ–PEO and linear PEO are different due to the differences in crystallization mechanism. In linear PEO, the crystallization is purely controlled by the nucleation mechanism. On the other hand, the diffusion-controlled mechanism predominates at the early stage of CSSQ–PEO crystallization whereas the nucleation-controlled mechanism is in the final stage of crystallization. The decrease in ΔE_a of CSSQ–PEO is consistent with the results shown in Fig. 2 that amplitude of the linear PEO peak is higher than that of CSSQ–PEO. The decrease in the activation energy of CSSQ–PEO can be hypothesized that the energy barrier for diffusion-controlled mechanism is lower than that of nucleation-controlled mechanism.

3.2. Crystallization morphology

The comparative study of the crystallization morphology between linear PEO and CSSQ–PEO was carried out by using cross-polarizing optical microscopy (CPOM). Fig. 8 shows the CPOM images of linear PEO (Fig. 8(a)–(c)) and CSSQ–PEO (Fig. 8(d)–(f)), both isothermally crystallized at 30 °C and the morphologies are developed in the early stage, the intermediates and the complete crystallization stage. It is clearly seen that the crystallites grow outward from the nucleus and appeared as a spherical shape at the early stage (Fig. 8(a)) and a progression of a growing spherulite is shown in Fig. 8(b). The color difference with the cross-polarizer corresponds to the rotation of the PEO chain orientation about the nucleus. The CPOM image of Fig. 8(c) shows the completion of PEO crystallization in a short period of time (~1 min). As seen in Fig. 8(d), a strong decrease of spherulite size of PEO with a definite boundary is observed in the presence of CSSQ. In addition, the nucleus size at the centre is obviously large that shows evidence for the CSSQ cage structure surrounded by the PEO nucleation. This observation is correlated with core-corona structure of CSSQ–PEO determined by TEM micrograph reported in our previous paper [29]. The completion of PEO crystallization is also observed at ~4 min [Fig. 8(d)] in CSSQ–PEO, which indicates the crystallization growth rate is slower compared to the linear PEO. The CPOM images substantiate the results obtained by DSC analysis. In addition, the spherulite structure of PEO inhibition by CSSQ allows the homogenous nucleation of large numbers of crystallites, which grow much smaller sizes than linear PEO spherulites as shown in Fig. 8. It is possible that the CSSQ core serves as a nucleating agent for the crystallization resulting in lower crystallinity compared to a linear PEO.

3.3. Wide-angle X-ray scattering (WAXS) studies

Fig. 9 shows the WAXS profiles of pure CSSQ, linear PEO and CSSQ–PEO, respectively. The spectrum of pure CSSQ shows many diffraction peaks at $2\theta = 18.8$, 19.5, 24.3, and 26.5°, revealing the rhombohedral unit structure of cubic silsesquioxane molecules [48]. The pattern of linear PEO is almost identical to the CSSQ–PEO spectrum except the intensities of the peaks are smaller in CSSQ–PEO. It is suggested that the presence of a small amount of cubic silsesquioxane cage inhibited the crystallization of PEO. The WAXS pattern of CSSQ at different cooling temperature was not detected due to the high melting temperature of CSSQ. The WAXS patterns for linear PEO and CSSQ–PEO on cooling from the melt are shown in Fig. 10. The profiles are taken near the crystallization temperature for both samples at a slow cooling rate (1 °C/min). It is noted that the diffraction peaks of

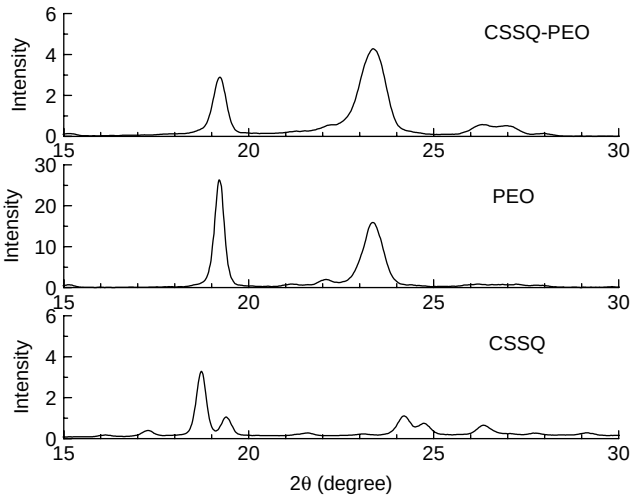

Fig. 9. WAXS profiles of pure CSSQ, linear PEO and CSSQ–PEO at room temperature.

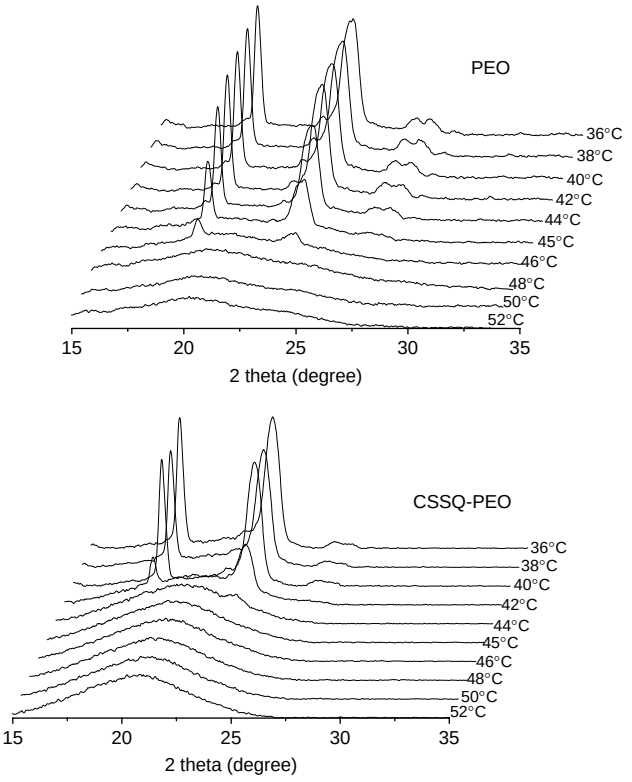

Fig. 10. WAXS spectra for linear PEO and CSSQ–PEO on cooling from the melt at a slow cooling rate (1 °C/min).

PEO appeared at 19.3 and 23.5° do not change in the WAXS spectrum of CSSQ–PEO indicating that there are no significant distortion of the crystal structure of PEO due to the presence of CSSQ. However, the diffraction peaks of PEO start appeared at 46 °C while the amorphous to crystallites transition of CSSQ–PEO is observed at 41 °C when cooled down from the melt. This is an evidence of the progressive slow crystallization of CSSQ–PEO as the cubic structure of CSSQ disturbs the crystallization process of PEO. This result is in agreement with the CPOM and DSC analysis, which exhibit the reduction of PEO crystallinity and the crystallization temperature decreased to 5–6 °C in the presence of CSSQ. Due to the small composition of CSSQ in CSSQ–PEO, the diffraction peaks contributed from CSSQ are not observed. Moreover, the diffraction peak at 24.3° in pure CSSQ spectrum diminished when CSSQ anchored with PEO chains.

4. Conclusion

Crystallization behavior of star-shaped CSSQ–PEO was investigated by DSC, cross-polarized optical microscopy, and WAXS analyses. As a comparison, we also studied the crystallization behavior of linear PEO. It was found that the glass transition temperature (T_g) of PEO increases from −34 to −25 °C, whereas the crystallization temperature (T_c) reduces from 34 to 28 °C in the presence of CSSQ. The nonisothermal crystallization kinetics of CSSQ–PEO and linear PEO were analyzed by Avrami and Ozawa methods. In the present study, the Avrami model does not adequately describe the non-isothermal crystallization kinetics of PEO and CSSQ–PEO. It was also found that the effect of molecular weight plays a role on the crystallization behavior, implying the low molecular weight of PEO crystallizes faster compared to the high molecular weight of PEO. On the other hand, the Ozawa method is qualitatively satisfactory for describing the nonisothermal crystallizations of PEO and CSSQ–PEO. It was observed the great dependence of the relative degree of crystallinity on the cooling rate at the initial stage of crystallization but slightly affected on the cooling rate at the end of the crystallization process. In linear PEO, the crystallization process is controlled by the nucleation mechanism. On the other hand, the diffusion-controlled mechanism predominates at the early stage of CSSQ–PEO crystallization whereas the nucleation-controlled mechanism is in the final stage of crystallization. The CPOM images indicated the crystallization growth rate is slower in CSSQ–PEO in comparison to the linear PEO. It was also investigated that more number of PEO spherulites in CSSQ–PEO were observed, which sizes are smaller than that of linear PEO spherulites. This suggests that the CSSQ serves as a nucleating agent for the crystallization resulting in lower crystallinity as supported by DSC analysis. WAXS spectra of linear PEO and CSSQ–PEO revealed that there is no change in crystal structure between linear PEO and star-shaped CSSQ–PEO although the crystallization growth rates are different.

Acknowledgements

We gratefully acknowledge financial support from the Institute of Materials, Research and Engineering (IMRE) under the Agency for Science, Technology, and Research (A*STAR), Singapore.

References

[1] Cebe P, Hong SD. Polymer 1986;27:1183.
[2] Dreezen G, Koch MHJ, Reynaers H, Groeninckx G. Polymer 1999;40:6451.
[3] Kong X, Tan S, Yang X, Li G, Zhou E, Ma D. J Polym Sci, Part B: Polym Phys 2000;38:3230.
[4] Wu L, Lisowski M, Talibuddin S, Runt J. Macromolecules 1999;32:1576.
[5] Cheng SZD, Wu SS, Chen J, Zhuo Q, Quirk RP. Macromolecules 1993;26:5105.
[6] Liu H, Yang G, He A, Wu M. J Appl Polym Sci 2004;94:819.
[7] Tjong SC, Bao SP. J Polym Sci, Part B: Polym Phys 2004;42:2878.
[8] Chen HL, Wu JC, Lin TL, Lin JS. Macromolecules 2001;34:6936.
[9] Liu X, Wu Q, Berglund LA, Qi Z. Macromol Mater Eng 2002;287:515.
[10] Krasteva M, Cerrada ML, Benavente R, Perez E. Polymer 2005;46:9831.
[11] Strawhecker KE, Manias E. Chem Mater 2003;15:844.
[12] Lee JC, Nakajima K, Ikehara T, Nishi T. J Appl Polym Sci 1997;64:797.
[13] Mi Y, Chen X, Guo Q. J Appl Polym Sci 1997;64:1267.
[14] Laine RM, Choi J, Lee I. Adv Mater 2001;13:800.
[15] Choi J, Haecup J, Yee AF, Zhu Q, Laine RM. J Am Chem Soc 2001;123:11420.
[16] Li GZ, Wang L, Tohiani H, Daulton TL, Koyama K, Pittman Jr CU. Macromolecules 2001;34:8686.
[17] Feher FJ, Budzichowski TA. J Organomet Chem 1989;379:33.
[18] Zhang C, Laine RM. J Am Chem Soc 2000;122:6979.
[19] Lichtenhan JD, Schwab JJ, Reinerth Sr WA. Chem Innovation 2001;1:3.
[20] Cheng H, Tamaki R, Laine RM, Babonneau F, Chujo Y, Treadwell DR. J Am Chem Soc 2000;122:10063.
[21] Lamm MH, Chen T, Glotzer SC. Nano Lett 2003;3:989.
[22] (a) Haddad TS, Lichtenhan JD. Macromolecules 1996;29:7302.
(b) Schwab JJ, Lichtenhan JD. Appl Organomet Chem 1998;12:707.
(c) Mather PT, Jeon HG, Romo-Uribe A, Haddad TS, Lichtenhan JD. Macromolecules 1999;32:1194.
[23] Dvornic PR, Hartmann-Thompson C, Keinath SE, Hill EJ. Macromolecules 2004;37:7818.
[24] Kim BS, Mather PT. Macromolecules 2002;35:8378.
[25] Maitra P, Wunder SL. Chem Mater 2002;14:4494.
[26] Capaldi FM, Rutledge GC, Boyce MC. Macromolecules 2005;38:6700.
[27] Patel RR, Mohanraj R, Pittman Jr CU. J Polym Sci, Part B: Polym Phys 2006;44:234.
[28] Bharadwaj RK, Berry RJ, Farmer BL. Polymer 2000;41:7209.
[29] Mya KY, Li X, Chen L, Ni X, Li J, He C. J Phys Chem B 2005;109:9455.
[30] Hao Q, Li F, Li Q, Li Y, Jia L, Yang J, et al. Biomacromolecules 2005;6:2236.
[31] Lang M, Wong RP, Chu C-C. J Polym Sci, Part A: Polym Chem 2002;40:1127.
[32] Lestel L, Cheradame H, Boileau S. Polymer 1990;31:1154.
[33] Hasegawa I, Motojima S. J Organomet Chem 1992;441:373.
[34] Gravel MC, Zhang C, Dinderman M, Laine RM. Appl Organomet Chem 1999;13:329.
[35] Allen RC, Mandelkern L. J Polym Sci, Part B: Polym Phys 1982;20:1465.
[36] Ozawa T. Polymer 1971;12:150.
[37] General Area Detector Diffraction System (GADDS) Manual, Bruker AXS Inc., Version 4.0; 1999.
[38] Bogdanov B, Vidts A, Van DBA, Verbeek R, Schacht E. Polymer 1998;39:1631.
[39] Choi J, Yee AF, Laine RM. Macromolecules 2003;36:5666.
[40] Hong S, Yang L, Macknight WJ, Gido SP. Macromolecules 2001;34:7009.

[41] Kong X, Yang X, Li G, Zhao X, Zhou E, Ma D. Eur Polym J 2001;37:1855.
[42] Beech DR, Booth C, Dodgson DV, Hillier IH. J Polym Sci, Part A-2 1972; 10:1555.
[43] Godovsky YK, Slonimsky GL, Garbar NM. In: Bailey Jr FE, Koleske JB, editors. Poly(ethylene oxide), Union Carbide Corporation. New York: Academic Press; 1976. p. 106.
[44] Qiu Z, Ikehara T, Nishi T. Polymer 2003;44:3101.
[45] Apiwanthanakorn N, Supaphol P, Nithitanakul M. Polym Test 2004;23: 817.
[46] Supaphol P, Apiwanthanakorn N. J Polym Sci, Part B: Polym Phys 2004; 42:4151.
[47] Kissinger HE. Anal Chem 1970;29:1702.
[48] Fu BX, Hsiao BS, Pagola S, Stephens P, White H, Rafailovich M, et al. Polymer 2001;42:599.